Series expansions for the massive Schwinger model in Hamiltonian lattice theory

C. J. Hamer,* Zheng Weihong,† and J. Oitmaa‡
School of Physics, The University of New South Wales, Sydney, NSW 2052, Australia
(Received 16 January 1997)

It is shown that detailed and accurate information about the mass spectrum of the massive Schwinger model can be obtained using the technique of strong-coupling series expansions. Extended strong-coupling series for the energy eigenvalues are calculated and extrapolated to the continuum limit by means of integrated differential approximants, which are matched onto a weak-coupling expansion. The numerical estimates are compared with exact results and finite-lattice results calculated for an equivalent lattice spin model with long-range interactions. Both the heavy fermion and the light fermion limits of the model are explored in some detail. [S0556-2821(97)04413-5]

PACS number(s): 11.15.Ha, 12.38.Gc

I. INTRODUCTION

The Schwinger model [1,2], or quantum electrodynamics in two space-time dimensions, has been a source of continuing interest over the years. It is a fascinating model in its own right, and also exhibits many of the same phenomena as QCD, such as confinement, chiral symmetry breaking with a U(1) axial anomaly, and a topological θ vacuum [3–5]. It is also perhaps the simplest nontrivial gauge theory, and this makes it a standard testbed for the trial of new techniques for the study of QCD.

Our main purpose in this paper is to explore the usefulness of the strong-coupling series approach to this model. It is well known that Euclidean Monte Carlo techniques have proved difficult and expensive to apply to models with dynamical fermions because of the infamous ''minus sign'' problem, and thus, it seems worthwhile to ask whether other techniques such as strong-coupling expansions can give useful information in such cases. Modern linked-cluster techniques [6] allow one to carry these expansions to very high order. We are particularly interested to see if the series approach can describe the nonrelativistic or heavy fermion limit of these models.

As a first test, we apply the approach to the Schwinger model, using a Hamiltonian lattice framework [7]. We concentrate on a calculation of the spectrum of bound states, more specifically the lowest two bound states, for the case of the massive Schwinger model. It will be shown that the series approach can give quite detailed and accurate information on the spectrum. It will be interesting to see if a similar approach is useful for models in higher dimensions.

Hamiltonian strong-coupling series were first calculated for the Schwinger model long ago by Banks, Kogut, and Susskind [7], and were extended by Carroll *et al.* [8]. Since then, however, the method has fallen into abeyance, being eclipsed by the power and accuracy of the Monte Carlo method.

Many other approaches have been made to the bound-state spectrum. In the massless case, of course, the model is exactly solvable, as shown by Schwinger [1,2]. It is equivalent to a theory of free, massive bosons. For a small fermion mass, one may perturb about the zero-mass limit, and obtain a low-mass expansion for the spectrum [8]. This expansion has recently been carried to second order by Vary *et al.* [9] and Adam [10]. In the large mass or nonrelativistic limit the ''positronium'' bound states can be solved in terms of a Schrödinger equation with a linear Coulomb potential [11]. For fixed, finite fermion mass, one has to resort to numerical techniques. A quite accurate variational calculation in the infinite momentum frame was performed by Bergknoff [12]. Finite-lattice Hamiltonian calculations were performed by Crewther and Hamer [13] and Irving and Thomas [14]: we include some further finite-lattice calculations in this paper, mainly as a check on the series results. Later on Eller, Pauli, and Brodsky [15] applied a ''discrete light-cone quantization'' (DLCQ) approach to the problem, and showed that it gave quite good results, not only for the lowest state, but for a whole range of higher excited states. Mo and Perry [16] have used a different light-front field theory approach, together with a Tamm-Dancoff approximation, which appears to give excellent results. Tomachi and Fujita [17] have used a ''Bogoliubov transformation method,'' which works quite well for small fermion masses.

In Sec. II of this paper the Hamiltonian lattice formulation of the model is reviewed, and the known analytic results on the bound-state spectrum are recalled. It is shown that for free boundary conditions the gauge degrees of freedom can be eliminated entirely from the lattice model, leading to an equivalent spin lattice model with long-range interactions. This is the formulation which we use to carry out the finite-lattice calculations.

Section III presents the numerical results. Their extrapolation to the continuum limit is discussed, and expansions near both the low-mass limit and the nonrelativistic limit are analyzed. The numerical results are compared with previous approaches. Finally our conclusions are summarized in Sec. IV.

II. FORMALISM

A. Continuum formulation

The continuum Lagrangian density takes the standard form

*Electronic address: c.hamer@unsw.edu.au
†Electronic address: w.zheng@unsw.edu.au
‡Electronic address: otja@newt.phys.unsw.edu.au

$$\mathcal{L}=-\frac{1}{4}F_{\mu\nu}F^{\mu\nu}+\overline{\psi}(i\partial\!\!\!/-gA\!\!\!/-m)\psi, \tag{1}$$

where

$$F_{\mu\nu}=\partial_\mu A_\nu-\partial_\nu A_\mu \tag{2}$$

and the Lorentz indices $\mu,\nu=0$ or 1. The coupling g in $1+1$ dimensions has the dimensions of mass. Choosing the time-like axial gauge

$$A_0=0 \tag{3}$$

the Hamiltonian is found to be

$$H=\int dx\left(-i\overline{\psi}\gamma^1(\partial_1+igA_1)\psi+m\overline{\psi}\psi+\frac{1}{2}E^2\right), \tag{4}$$

where the electric field E has only one component in one spatial dimension:

$$E=F^{10}=-\dot{A}^1. \tag{5}$$

The remaining gauge component is not an independent degree of freedom, but can be eliminated if desired, using the constraint provided by the equation of motion (Gauss' law):

$$\partial_1 E=-\partial_1\dot{A}^1=g\overline{\psi}\gamma^0\psi. \tag{6}$$

In the massless case, the theory has been solved by Schwinger [1,2], and becomes equivalent to a theory of free, massive bosons, with mass

$$\frac{M_1}{g}=\frac{1}{\sqrt{\pi}}\simeq 0.564. \tag{7}$$

For small electron mass m/g, one can obtain analytic estimates by perturbing about the massless limit. Caroll, Kogut, Sinclair, and Susskind [8] found that the lowest-mass (''vector'') state has mass

$$\frac{M_1}{g}=\frac{1}{\sqrt{\pi}}+e^{\gamma}\left(\frac{m}{g}\right)+\cdots\simeq 0.564+1.78\left(\frac{m}{g}\right)+\cdots, \tag{8}$$

while the ratio of the next-lowest (''scalar'') mass to the vector mass was

$$\frac{M_2}{M_1}=2-2\pi^3 e^{2\gamma}\left(\frac{m}{g}\right)^2+\cdots\simeq 2-197\left(\frac{m}{g}\right)^2+\cdots, \tag{9}$$

where $\gamma\simeq 0.5772\cdots$ is Euler's constant.

These results have been extended to second order by Vary, Fields, and Pirner [9] and by Adam [10]:

$$\frac{M_1}{g}=0.5642+1.781\left(\frac{m}{g}\right)+0.1907\left(\frac{m}{g}\right)^2+\cdots. \tag{10}$$

Adam [10] also found

$$\frac{M_2}{M_1}=2-\frac{\pi^3 e^{2\gamma}}{64}\left(\frac{m}{g}\right)^2+\cdots\simeq 2-1.5368\left(\frac{m}{g}\right)^2+\cdots \tag{11}$$

differing from the result of Carroll *et al.* [8] by a factor of $2^7=128$.

In the large-mass or nonrelativistic limit, the ''positronium'' bound states are described by a Schrödinger equation with a linear potential [11],

$$\left(\frac{p^2}{m}+\frac{1}{2}g^2|x|\right)\Psi(x)=E\Psi(x), \tag{12}$$

where the nonrelativistic energy is

$$E=M-2m. \tag{13}$$

Equation (12) may be solved in terms of Airy functions, to give the energies of the lowest vector and scalar states as [11]

$$\begin{aligned}\frac{E_1}{g}&\sim 0.642\left(\frac{g}{m}\right)^{1/3}\quad \text{as } m/g\to\infty,\\ \frac{E_2}{g}&\sim 1.473\left(\frac{g}{m}\right)^{1/3}\quad \text{as } m/g\to\infty.\end{aligned} \tag{14}$$

B. Lattice formulation

The model can now be formulated on a ''staggered'' spatial lattice [7]. Let the lattice spacing be a, and label the sites with an integer n. Define a single-component fermion field $\phi(n)$ at each site n, obeying anticommutation relations:

$$\{\phi^\dagger(n),\phi(m)\}=\delta_{mn},\quad \{\phi(n),\phi(m)\}=0. \tag{15}$$

The gauge field is defined on the links $(n,n+1)$ connecting each pair of sites by

$$U(n,n+1)=e^{i\theta(n)}=e^{-iagA^1(n)}. \tag{16}$$

Then the lattice Hamiltonian equivalent to Eq. (4) is

$$\begin{aligned}H=&-\frac{i}{2a}\sum_{n=1}^{N}\left[\phi^\dagger(n)e^{i\theta(n)}\phi(n+1)-\text{H.c.}\right]\\ &+m\sum_{n=1}^{N}(-1)^n\phi^\dagger(n)\phi(n)+\frac{g^2a}{2}\sum_{n=1}^{N}L^2(n),\end{aligned} \tag{17}$$

where the number of lattice sites N is even, and the correspondence between lattice and continuum fields is

$$\phi(n)/\sqrt{a}\to\begin{cases}\psi_{\text{upper}}(x), & n \text{ even},\\ \psi_{\text{lower}}(x), & n \text{ odd}\end{cases} \tag{18}$$

(''upper'' and ''lower'' being the two components of the continuum spinor), and

$$\begin{aligned}\frac{1}{ag}\theta(n)&\to -A^1(x),\\ gL(n)&\to E(x).\end{aligned} \tag{19}$$

The γ matrices are represented by

$$\gamma^0=\begin{pmatrix}1 & 0\\ 0 & -1\end{pmatrix},\quad \gamma^1=\begin{pmatrix}0 & 1\\ -1 & 0\end{pmatrix}. \tag{20}$$

As usual, we have chosen a ''compact'' formulation where the gauge field becomes an angular variable on the lattice, and $L(n)$ is the conjugate ''spin'' variable

$$[\theta(n),L(m)]=i\delta_{nm}, \tag{21}$$

so that $L(n)$ has integer eigenvalues $L(n)=0,\pm1,\pm2,\ldots$. As noted by Banks *et al.* [7], this quantization of electric field (or flux) in one dimension also occurs in the continuum Schwinger model, due to Gauss' law. If one takes the naive continuum limit $a\to0$, the lattice Hamiltonian (17) reduces to the continuum Hamiltonian (4), as it should.

Now define the dimensionless operator

$$W=\frac{2}{ag^2}H=W_0+xV, \tag{22}$$

where

$$W_0=\sum_n L^2(n)+\mu\sum_n (-1)^n\phi^\dagger(n)\phi(n), \tag{23}$$

$$V=-i\sum_n [\phi^\dagger(n)e^{i\theta(n)}\phi(n+1)-\text{H.c.}], \tag{24}$$

$$\mu=\frac{2m}{g^2a},\quad x=\frac{1}{g^2a^2}. \tag{25}$$

For $x\ll1$ one can employ strong-coupling perturbation theory on this model, treating W_0 as the unperturbed Hamiltonian and V as the perturbation, as discussed by Banks *et al.* [7]. In the strong-coupling limit, the unperturbed ground state $|0\rangle$ is the eigenstate with

$$L(n)=0,\quad \phi^\dagger(n)\phi(n)=\frac{1}{2}[1-(-1)^n]\quad \text{all } n \tag{26}$$

whose energy will be normalized to zero, corresponding to a ''filled Dirac sea.'' Banks *et al.* [7] have discussed how to use Rayleigh-Schrödinger perturbation theory to generate perturbation series in x for the ground state and excited state eigenvalues of this system, and the discussion will not be repeated here. We have used more sophisticated linked-cluster techniques [6] to generate high-order perturbation series for these eigenvalues, as presented below.

The lattice version of Gauss' law is then taken as

$$L(n)-L(n-1)=\phi^\dagger(n)\phi(n)-\frac{1}{2}[1-(-1)^n], \tag{27}$$

which means excitations on odd and even sites create ∓1 units of flux, corresponding to ''electron'' and ''positron'' excitations, respectively.

C. Equivalent spin formulation

The one-component fermion operators can be replaced by Pauli spin operators at each site if we employ a Jordan-Wigner transformation [7],

$$\phi(n)=\prod_{l<n}[i\sigma_3(l)]\sigma^-(n), \tag{28}$$

$$\phi^\dagger(n)=\prod_{l<n}[-i\sigma_3(l)]\sigma^+(n), \tag{29}$$

giving

$$W_0=\sum_n L^2(n)+\frac{\mu}{2}\sum_n (-1)^n\sigma_3(n)+N\mu/2, \tag{30}$$

$$V=\sum_n [\sigma^+(n)e^{i\theta(n)}\sigma^-(n+1)+\text{H.c.}]. \tag{31}$$

The strong-coupling ground state then corresponds to

$$L(n)=0,\quad \sigma_3(n)=-(-1)^n\quad \text{all } n. \tag{32}$$

Next, the gauge field can be eliminated using Gauss' law,

$$L(n)-L(n-1)=\frac{1}{2}[\sigma_3(n)+(-1)^n], \tag{33}$$

and a residual gauge transformation

$$\sigma^-(n)\to\prod_{l<n}\{e^{-i\theta(l)}\}\sigma^-(n) \tag{34}$$

provided that we assume free boundaries

$$L(0)=L(N)=0\quad \text{where } N=\text{No. lattice sites}. \tag{35}$$

(If periodic boundary conditions are assumed, then there is one extra independent gauge degree of freedom left over, corresponding to the ''background'' electric field [4].) The resulting Hamiltonian is then

$$W=W_0+xV, \tag{36}$$

where

$$W_0=\frac{\mu}{2}\sum_{n=1}^{N}(-1)^n\sigma_3(n)+\frac{N\mu}{2}+\sum_{n=1}^{N-1}\left[\frac{1}{2}\sum_{m=1}^{n}[\sigma_3(m)+(-1)^m]\right]^2, \tag{37}$$

$$V=\sum_{n=1}^{N-1}[\sigma^+(n)\sigma^-(n+1)+\text{H.c.}]. \tag{38}$$

All trace of the gauge field has now disappeared, but instead there is a nonlocal, long-range interaction between the spins in the last term of Eq. (37), which of course corresponds to the long-range Coulomb interaction between charges in the original theory. In the continuum limit $a\to0$, $x\to\infty$, the interaction V dominates the Hamiltonian so that in leading order the system becomes equivalent to a simple XY model with ground-state energy per site

$$\frac{\omega_0}{N}\to-\frac{x}{\pi}\quad \text{as } x\to\infty. \tag{39}$$

The energy gap to the lowest excited state in the sector of ''vector'' states will correspond to the vector mass, so we expect

$$\omega_1-\omega_0=\frac{2}{ag^2}M_1=\frac{2}{g}M_1\sqrt{x} \tag{40}$$

and similarly in the scalar or ground-state sector, the minimum energy gap

$$\omega_2-\omega_0=\frac{2}{ag^2}M_2=\frac{2}{g}M_2\sqrt{x}. \tag{41}$$

Our aim in this paper is to find estimates of these masses M_1 and M_2.

The equivalent spin model has a total of only 2^N possible configurations, and lends itself readily to finite-lattice techniques of analysis. As a check on the series results, we have used the Lanczos algorithm to obtain exact results for the low-lying eigenvalues of this system at finite x on lattices of up to $N=22$ sites. The ground state energy ω_0 is easily obtained as the lowest eigenvalue in the sector containing the unperturbed ground state $|0\rangle$; and the first excited state energy ω_1 is likewise the lowest eigenvalue in the ''vector'' state sector, corresponding in the strong-coupling limit to the state [7]

$$|1\rangle=\frac{1}{\sqrt{N}}\sum_{n-1}^{N-1}[\sigma^+(n)\sigma^-(n+1)-\text{H.c.}]|0\rangle. \tag{42}$$

The second excited-state energy ω_2 is the lowest of a ''band'' of excited states in the vacuum sector, corresponding in the strong-coupling limit to the state

$$|2\rangle=\frac{1}{\sqrt{N}}\sum_{n=1}^{N-1}[\sigma^+(n)\sigma^-(n+1)+\text{H.c.}]|0\rangle. \tag{43}$$

III. RESULTS AND ANALYSIS

A. Finite-lattice results

Exact eigenvalues have been calculated for the equivalent spin Hamiltonian (36) using the Lanczos technique for various values of m/g and coupling x, on even lattices from $N=4$ up to $N=22$ sites. No symmetrization of states was employed: since free boundary conditions were chosen, the system does not exhibit translational invariance in any case. The calculations are carried out in the sector $\Sigma_i\sigma_3(i)=0$ which has $N!/[(N/2)!]^2$ states, and the ground-state energy ω_0 and the ''vector'' excited-state energy ω_1 are the lowest and the second lowest eigenvalues in this sector, respectively. The ''scalar'' excited-state energy ω_2 is slightly more tricky to obtain because there are several other states, corresponding to the momentum excitations of the ''vector'' excited state, in this sector giving lower energy than the ''scalar'' excited state. We got over this problem by moving in stages from the strong-coupling limit $x=0$ to the desired coupling value, and ''tagging'' the desired state as that which has maximum overlap with its predecessor at each stage, starting from the state $|2\rangle$ in Eq. (43).

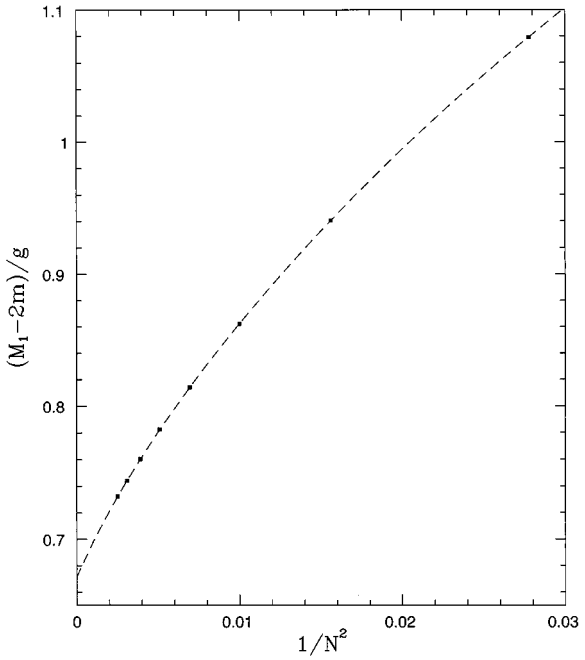

FIG. 1. Finite-size scaling behavior of the vector energy gap $(M_1-2m)/g$ as a function of $1/N^2$ for $m/g=0$, $x=4$, where N is the lattice size. Solid boxes mark the finite-lattice data points; the dashed line shows a polynomial fit of the form (45).

To make comparison with series data, it is first necessary to extrapolate the finite-lattice data to the bulk limit $N\to\infty$. The convergence of the finite-lattice sequences was slow. Tests showed that the convergence was polynomial in $1/N$: thus for the ground-state energy

$$\omega_0(N)\to N\epsilon_0(\infty)+b_0+\frac{b_1}{N^2}+O(N^{-3}) \quad \text{as } N\to\infty, \tag{44}$$

where $\epsilon_0(\infty)$ is the bulk energy per site and b_0 is the surface energy term; while for the energy gaps

$$\omega_i(N)-\omega_0(N)\to b_0'+\frac{b_1'}{N^2}+O(N^{-3}) \quad \text{as } N\to\infty. \tag{45}$$

This is opposed to the exponential convergence $\sim\exp(-cN)$ one normally expects for periodic boundary conditions. There is a simple explanation for this behavior:[1] on the lattice with free boundaries, the excitations have finite momentum $O(\pi/N)$, and thus their energies include a kinetic energy correction term $O((\pi/N)^2)$. As one approaches $x\to\infty$, which is a critical point of the lattice model, the finite-lattice corrections become relatively much larger, and extrapolation to the bulk limit becomes progressively more difficult. An example is shown in Fig. 1 for $x=4$, $m/g=0$.

Various sequence extrapolation algorithms [18–20] were tried for estimating the bulk limit, such as the alternating VBS algorithm, and the Lubkin and Bulirsch-Stoer algorithms, but the most reliable and accurate method in this case

[1]We are indebted to Dr. O. Sushkov for this remark.

TABLE I. Series coefficients in x for the series f_0, f_1, f_2, and f_3 for the vector and scalar excited states. Nonzero coefficients of x^n are listed.

n	f_0	f_1	f_2	f_3
		Vector excited state		
0	1.000000000000	0.000000000000	0.000000000000	0.000000000000
2	2.000000000000	-4.000000000000	8.000000000000	$-1.600000000000\times10^{1}$
4	$-1.000000000000\times10^{1}$	$5.600000000000\times10^{1}$	$-2.160000000000\times10^{2}$	$7.040000000000\times10^{2}$
6	$7.866666666667\times10^{1}$	$-7.484444444444\times10^{2}$	$4.344296296296\times10^{3}$	$-1.979753086420\times10^{4}$
8	$-7.362222222222\times10^{2}$	$9.942962962963\times10^{3}$	$-7.742029629630\times10^{4}$	$4.547973004115\times10^{5}$
10	$7.572929100529\times10^{3}$	$-1.326103683144\times10^{5}$	$1.296902835617\times10^{6}$	$-9.337217941993\times10^{6}$
12	$-8.273669056689\times10^{4}$	$1.780034473768\times10^{6}$	$-2.096087983379\times10^{7}$	$1.787437096185\times10^{8}$
14	$9.428034196036\times10^{5}$	$-2.405247329390\times10^{7}$	$3.312148486580\times10^{8}$	$-3.264352340840\times10^{9}$
16	$-1.108357531764\times10^{7}$	$3.269962317907\times10^{8}$	$-5.154702578031\times10^{9}$	$5.764697147243\times10^{10}$
18	$1.334636403738\times10^{8}$	$-4.469545711783\times10^{9}$	$7.935843765541\times10^{10}$	$-9.927975671713\times10^{11}$
20	$-1.637995781331\times10^{9}$	$6.137741867815\times10^{10}$	$-1.211925759935\times10^{12}$	$1.676878382095\times10^{13}$
22	$2.041592824001\times10^{10}$	$-8.462460202654\times10^{11}$	$1.839263212769\times10^{13}$	$-2.788695534036\times10^{14}$
24	$-2.577314968112\times10^{11}$	$1.170804957950\times10^{13}$	$-2.777427143130\times10^{14}$	$4.579160745014\times10^{15}$
26	$3.288641969992\times10^{12}$	$-1.624677659161\times10^{14}$	$4.176990920608\times10^{15}$	$-7.439926786605\times10^{16}$
28	$-4.234675197596\times10^{13}$	$2.260335118290\times10^{15}$	$-6.260315585321\times10^{16}$	$1.197974308422\times10^{18}$
		Scalar excited state		
0	1.000000000000	0.000000000000	0.000000000000	0.000000000000
2	6.000000000000	$-1.200000000000\times10^{1}$	$2.400000000000\times10^{1}$	$-4.800000000000\times10^{1}$
4	$-2.600000000000\times10^{1}$	$1.520000000000\times10^{2}$	$-6.000000000000\times10^{2}$	$1.984000000000\times10^{3}$
6	$1.906666666667\times10^{2}$	$-1.884444444444\times10^{3}$	$1.120829629630\times10^{4}$	$-5.195753086420\times10^{4}$
8	$-1.756666666667\times10^{3}$	$2.435066666667\times10^{4}$	$-1.932472592593\times10^{5}$	$1.151850271605\times10^{6}$
10	$1.804833650794\times10^{4}$	$-3.218263683144\times10^{5}$	$3.192825551667\times10^{6}$	$-2.325598645777\times10^{7}$
12	$-1.979052000756\times10^{5}$	$4.314452729791\times10^{6}$	$-5.136573365113\times10^{7}$	$4.420974571815\times10^{8}$
14	$2.267367521095\times10^{6}$	$-5.842838007004\times10^{7}$	$8.115577786905\times10^{8}$	$-8.058540815871\times10^{9}$
16	$-2.681007957489\times10^{7}$	$7.972653477157\times10^{8}$	$-1.265571251416\times10^{10}$	$1.424081244509\times10^{11}$
18	$3.246557142476\times10^{8}$	$-1.094270467476\times10^{10}$	$1.954139217902\times10^{11}$	$-2.457363530118\times10^{12}$
20	$-4.005343740541\times10^{9}$	$1.508952103990\times10^{11}$	$-2.994043095570\times10^{12}$	$4.161067716407\times10^{13}$
22	$5.016016326942\times10^{10}$	$-2.088733926173\times10^{12}$	$4.558824467106\times10^{13}$	$-6.938732610121\times10^{14}$
24	$-6.359434181405\times10^{11}$	$2.900477258173\times10^{13}$	$-6.905937254404\times10^{14}$	$1.142452124172\times10^{16}$
26	$8.145971243132\times10^{12}$	$-4.038508440296\times10^{14}$	$1.041673344896\times10^{16}$	$-1.861014699378\times10^{17}$

seemed to be a simple least squares polynomial fit in $1/N$, with fictitious errors assigned to the data points. Consistency between the estimates at different orders allows a crude estimate of the likely error in the final result. This was the technique used to obtain the estimates used in the rest of this paper.

B. Series expansions

Strong-coupling perturbation series have been calculated for the ground-state energy ω_0, and the energy gaps $(\omega_1-\omega_0)$ and $(\omega_2-\omega_0)$, as functions of the coupling x and mass parameter μ. The full series up to order x^{10} are presented in the Appendix.

These series can be analyzed in three different regimes, as follows.

1. Massless limit, $m/g\to0$

For small m/g, the eigenvalues can be expanded as series in the mass parameter μ, e.g., for the vector gap

$$(\omega_1-\omega_0)[x,\mu]-2\mu=f_0(x)+\mu f_1(x)+\mu^2 f_2(x)+\cdots. \tag{46}$$

The series have been calculated for $f_i(x)$ $(i=0,1,\ldots,6)$ up to order x^{28} for the vector excited state and order x^{26} for the scalar excited state. Coefficients for the series $f_i(x)$ $(i=0,1,2,3)$ are listed in Table I. The expected behavior in the continuum limit for these series is

$$f_l(x)\to a_l x^{(1-l)/2} \quad \text{as} \quad x\to\infty \tag{47}$$

which would lead to a continuum energy gap

$$\frac{M-2m}{g}=a_0/2+a_1(m/g)+2a_2(m/g)^2+\cdots. \tag{48}$$

These series must now be extrapolated from the strong-coupling limit $x=0$ to the continuum limit $x\to\infty$. We have employed the standard techniques of integrated differential approximants and naive Padé approximants [20] for this purpose, combined with a ''matching'' technique. Some examples are shown in Figs. 2, 3, and 4.

The integrated differential approximants are a natural generalization of the Padé approximant, and can approximate

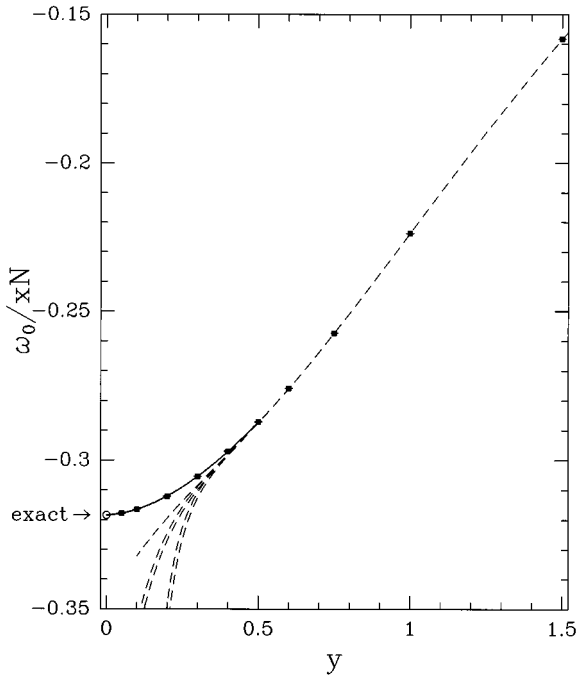

FIG. 2. Ground-state energy per site $\omega_0/(xN)$ as a function of $y=1/\sqrt{x}$ for $m/g=0$. The dashed lines are integrated differential approximants to the series data, while the solid boxes with error bars represent finite-lattice estimates. The solid line is a fit to the finite-lattice data in powers of y. The exact continuum limit is marked by an open circle.

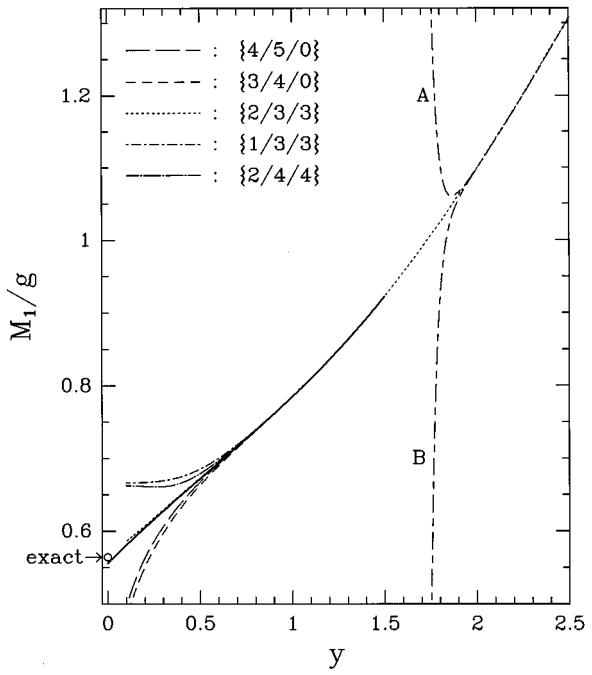

FIG. 3. Vector mass gap M_1/g as a function of $y=1/\sqrt{x}$ for $m/g=0$. The open circle marks the exact continuum limit. Dashed lines are the $\{m/l/k\}$ order integrated differential approximants to the series $(\omega_1-\omega_0)^4$. Shown also are the naive sum to order x^{26} (labeled by A) and x^{28} (labeled by B), and the third-order weak-coupling fit to the series data over the range $[0.7,1.5]$ in y (the solid line).

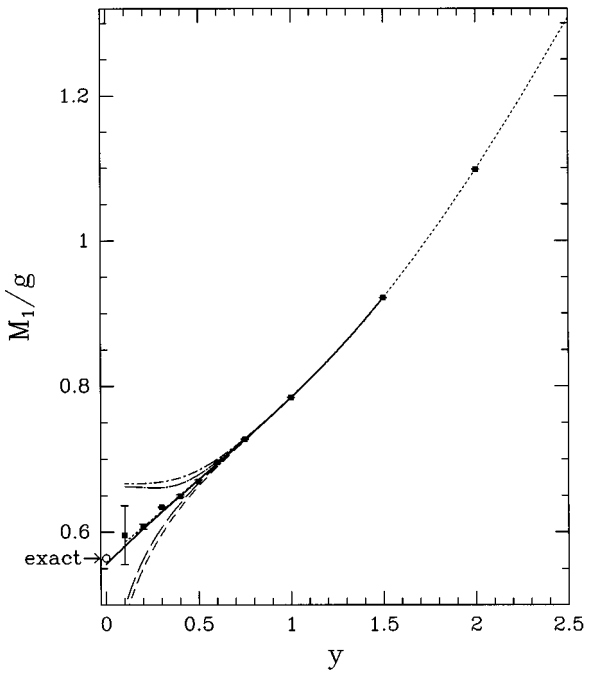

FIG. 4. As Fig. 3, with finite-lattice data included (solid boxes).

more general types of singularities [20]. The $\{m/l/k\}$ first-order inhomogeneous differential approximant [20] to a function

$$f(z)=\sum_{n\geqslant 0} a_n z^n$$

is a function of polynomials P_l, Q_m, and R_k of degree l, m, and k, respectively, satisfying the differential equation

$$P_l(z)\frac{df(z)}{dz}+Q_m(z)f(z)+R_k(z)=0(z^{l+m+k+2}). \quad (49)$$

Once P_l, Q_m, and R_k are determined order by order from Eq. (49), the approximant is the function which satisfies Eq. (49) with the right-hand side replaced by zero. It may be found by numerical integration.

Figure 2 shows the ground-state energy per site for $m/g=0$ as a function of $y=1/\sqrt{x}$ (which is the natural variable to use at weak couplings, as shown by Eq. (47) and by previous weak-coupling analyses [11,21]). It can be seen that the approximants converge down to about $y\simeq 0.5$, and are in excellent agreement with the finite-lattice estimates. These can easily be extrapolated to the continuum limit $x=0$, where

$$\frac{\omega_0}{Nx}=-\frac{1}{\pi} \quad (50)$$

according to Eq. (39).

A more interesting example is seen in Fig. 3, which shows the series data for the vector energy gap as a function of y. It can be seen that the raw series begins to diverge below about $y\simeq 1.9$. A more useful technique is to analytically continue the series by means of integrated differential approximants [20]. In view of the fact that the series involves powers of

x^2, and the asymptotic behavior of $(\omega_1-\omega_0)$ is given by Eq. (40), approximants were actually calculated for the function $(\omega_1-\omega_0)^4$. They converge much better than the raw series, down to about $y\simeq 0.7$, and spray outwards somewhat below that. The higher-order approximants usually converge deeper into the weak-coupling region, but the improvement is not very dramatic as the order is increased. One still has to make an extrapolation to the continuum limit $y=0$.

Now in the weak-coupling region, the function is expected to have an asymptotic expansion [11,21]

$$\frac{M_1}{g}=\sum_{n=0}^{\infty} c_n y^n + O(e^{-b/y}). \tag{51}$$

Figure 3 shows that the function is smooth and well behaved over the region $0.7\leqslant y\leqslant 1.5$, and can be well fitted by a low-order polynomial in y of the form (51) (ignoring any exponentially small correction terms). Such a polynomial fit is shown as a solid line in Fig. 3. It extrapolates to a value

$$\frac{M_1}{g}\to 0.56(2) \quad \text{as } y\to 0, \tag{52}$$

where the error is crudely estimated from the difference between the second-order and third-order fits. This result compares well with the expected exact value of 0.5642 obtained from Eqs. (8) and (40). A reliable estimate of the continuum limit has thus been obtained by ''matching'' a weak-coupling polynomial form with the series approximant data over a ''window'' of intermediate couplings ($0.7\leqslant y\leqslant 1.5$, in this case), which is presumed to be in the weak-coupling region. A similar matching technique was used previously on finite-lattice data by Crewther and Hamer [13] and Irving and Thomas [14], and is also common in lattice Monte Carlo studies. We have also used it previously in a series study of the U(1) Yang-Mills theory in (2+1) dimensions [22].

Figure 4 is similar to Fig. 3, but with the finite-lattice estimates added. It can be seen that the weak-coupling fit to the series data agrees well with the finite-lattice data, confirming that this method of extrapolation is reliable. A fit to the finite-lattice data gives an even more accurate estimate of the continuum limit:

$$\frac{M_1}{g}\to 0.57(1) \quad \text{as } y\to 0. \tag{53}$$

Figure 5 is a similar plot for the energy of the scalar excited state. Here it can be seen that the series approximants converge down to $y\simeq 1$, where the function develops a pronounced peak or bump. It is not really possible to tell from the diverging series approximants whether the function increases, decreases, or remains flat below that point, but the finite-lattice data show that it decreases gently towards the exact continuum value 1.128. A fit to the finite-lattice data over 0.2–0.8 in y gives

$$\frac{M_2}{g}\to 1.14(3) \quad \text{as } y\to 0 \tag{54}$$

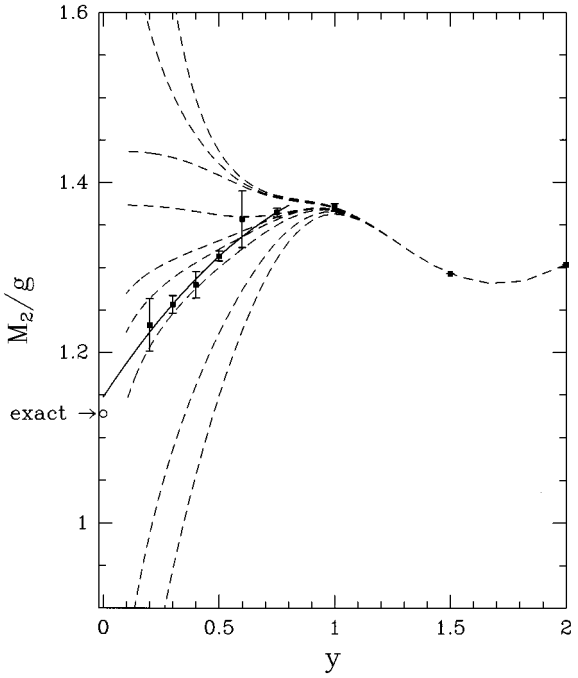

FIG. 5. Scalar mass gap M_2/g as a function of $y=1/\sqrt{x}$, for $m/g=0$, notation as in Fig. 3. Here the solid line represents a second-order polynomial fit to the finite-lattice data over the range [0.2,0.8] in y.

in quite reasonable agreement with the exact value; but the best one could do with the series data would be to estimate a qualitative value,

$$a_0^{\text{scalar}}\simeq 1.25(15). \tag{55}$$

In a similar fashion, estimates have been obtained for the coefficients a_0, a_1, a_2, a_3, in Eq. (48) for the vector and scalar masses, extracted from both the series data and the finite-lattice data. These are summarized in Table II, along with the exact results (where known). It can be seen that the numerical estimates are in good agreement with the exact results for the vector state. The series results are actually competitive with or better than the finite-lattice results for the higher coefficients, and thus give a detailed picture of the behaviour of the vector energy gap at low fermion mass m. The estimate for a_3 should also be fairly reliable for this state, and it would be interesting to check it against analytic

TABLE II. Table of estimates of a_0, $a_1,\ldots,a_3$ for the vector and scalar masses, obtained from series data, finite-lattice data, and exact results [9,10].

	$a_0/2$	a_1+2	$2a_2$	$4a_3$
		Vector state		
Series	0.56(2)	1.80(2)	0.16(4)	−0.22(6)
Finite lattice	0.57(1)	1.78(2)	0.3(1)	
Exact	0.5642	1.781	0.1908	
		Scalar state		
Series	1.25(15)	3.2(2)	−4(2)	
Finite lattice	1.14(3)	2.5(10)	0(2)	
Exact	1.1284	3.562	−0.485	

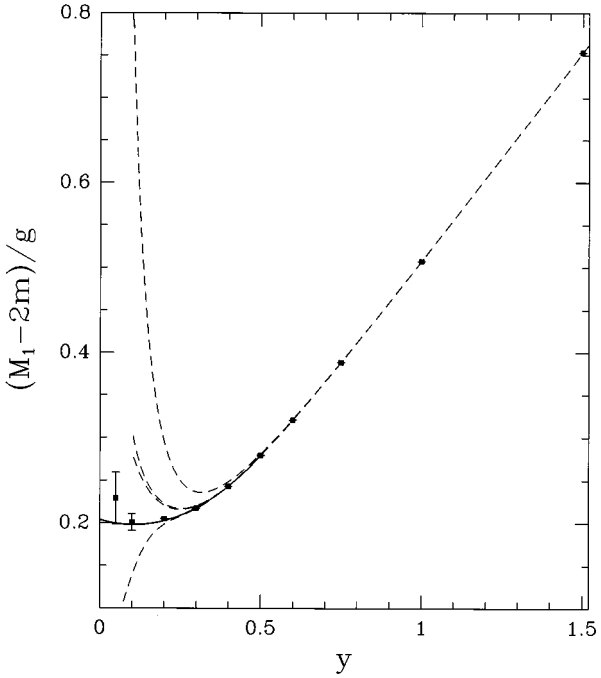

FIG. 6. The vector energy gap $(M_1-2m)/g$ as a function of $y=1/\sqrt{x}$ for $m/g=32$, notation as in Fig. 4. Here the solid line represents a second-order polynomial fit to the finite-lattice data over the range [0–0.5] in y.

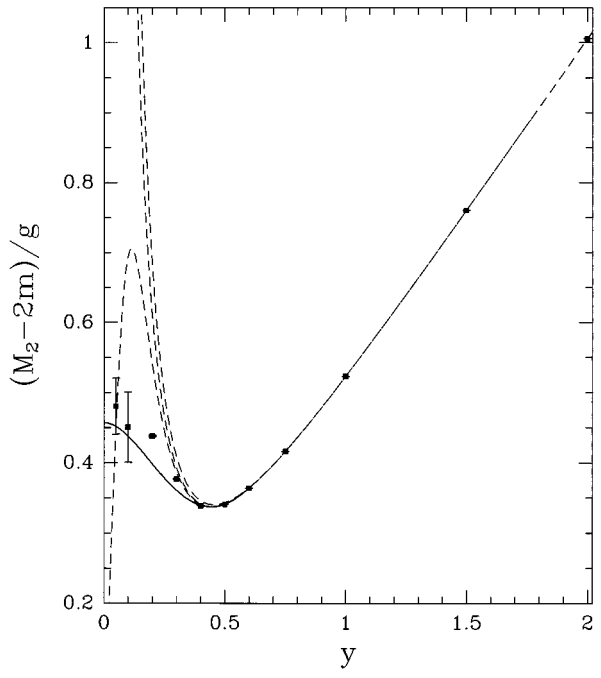

FIG. 7. The scalar energy gap $(M_2-2m)/g$ as a function of $y=1/\sqrt{x}$ for $m/g=32$, notation as in Fig. 4. Here the solid line represents a polynomial fit to the finite-lattice data over the range [0–0.7] in y.

calculations. For the scalar state, there is more structure at small y, as seen in Fig. 5, and although the estimates for a_0 and a_1 agree quite well with the exact results, those for a_2 and a_3 are virtually worthless.

2. Finite m/g

At fixed, finite m/g, the series have been calculated up to order x^{30} for the ground-state energy ω_0, and order $x^{53/2}$ for the energy gaps $(\omega_1-\omega_0)$ and $(\omega_2-\omega_0)$—these series are available on request. The analysis follows very similar lines to those described above. The major difference is that for $m/g\neq 0$, the strong-coupling series expansions are in powers of $x^{1/2}$, rather than x^2. The series are therefore longer, but the convergence is not very different to that at $m/g=0$.

At large m/g the series coefficients begin to grow very rapidly, like $(m/g)^n$ at large orders n, and it becomes more difficult to maintain good accuracy down to small values of y. Figures 6 and 7 illustrate the behavior of the energy gap at large m/g. It can be seen that any structure has moved to smaller values of y, and is somewhat less pronounced than at $m/g=0$.

Our estimates of the energies E_i/g are shown in Table III and Fig. 8, along with earlier finite-lattice estimates of Crewther and Hamer [13], and the light-cone estimates of Eller *et al.* [15] and Mo and Perry [16]. It can be seen that all the estimates agree with each other, within errors, except that the results of Eller *et al.* [15] run a little too high at small m/g. For the vector state, the data match beautifully to the asymptotic expansions at both ends. For the scalar state, the data indicate a peak in the energy at about $m/g\simeq 0.5$.

Comparing the different estimates, it is noticeable that our current finite-lattice estimates are in fact less accurate than the old estimates of Crewther and Hamer [13] or the even more accurate results of Irving and Thomas [14], although there is good consistency between them. This is because of the large finite-size corrections associated with the free boundary conditions. More importantly, the series estimates are seen to be in good agreement with the current finite-lattice estimates, and for the vector state they are generally almost as accurate (approximately 10%), although for the scalar state they are worse (approximately 15–20%). The results of Mo and Perry [16] seem very reliable and accurate, but unfortunately there is no assessment of the likely errors in their results.

3. Nonrelativistic limit, m/g→∞

At large m/g, a natural rearrangement of the series for the energy gaps was suggested by Hamer [11]. Instead of variables μ and x, one can rearrange the series in terms of variables $1/\mu$ and u, where

$$u=\frac{x^2}{\mu}=\frac{1}{2mg^2a^3}=\frac{1}{2m/g}x^{3/2}. \tag{56}$$

Then one finds the series can easily be expanded in powers of the inverse mass parameter $1/\mu$, e.g., for the vector gap

$$(\omega_1-\omega_0)[u,\mu]-2\mu=\tilde{f}_0(u)+\frac{1}{\mu}\tilde{f}_1(u)+\frac{1}{\mu^2}\tilde{f}_2(u)+\cdots. \tag{57}$$

The continuum limit can then be approached by first letting m/g (or μ) $\to\infty$ in such a way that mg^2 (or u) remains finite, and then letting $a\to 0$, or $u\to\infty$. If we *assume* that each separate term on the right-hand side of Eq. (57) gives a

TABLE III. Estimates of the continuum bound-state energies E_1/g, E_2/g as functions of m/g. The series and finite-lattice estimates obtained in this work are compared with the earlier finite-lattice estimates of Crewther and Hamer [13], and the light-cone estimates of Eller *et al.* [15] and Mo and Perry [16].

m/g	Series This work	Finite lattice This work	CH [13]	Eller *et al.* [15]	Mo and Perry [16]
			Vector state		
0	0.56(2)	0.57(1)	0.56(1)		
0.125	0.53(3)	0.52(2)	0.54(1)	0.60	0.54
0.25	0.52(4)	0.52(2)	0.52(1)	0.53	0.52
0.5	0.50(2)	0.50(2)	0.50(1)	0.49	0.49
1	0.46(4)	0.46(3)	0.46(1)	0.44	0.44
2	0.41(4)	0.41(3)	0.413(5)	0.39	0.39
4	0.34(2)	0.35(2)	0.358(5)	0.34	0.34
8	0.30(3)	0.31(2)	0.299(5)	0.28	0.29
16	0.24(3)	0.25(2)	0.245(5)	0.23	0.24
32	0.20(4)	0.20(2)	0.197(5)	0.20	0.20
			Scalar state		
0	1.25(15)	1.14(3)	1.12(5)		
0.125	1.35(15)	1.24(4)	1.11(5)	1.41	1.22
0.25	1.30(15)	1.27(5)	1.12(5)	1.31	1.23
0.5	1.25(15)	1.25(5)	1.15(5)	1.23	1.20
1	1.10(15)	1.14(5)	1.19(5)	1.13	1.12
2	1.00(15)	1.01(5)	1.10(5)	0.98	0.99
4	0.90(15)	0.85(4)	0.93(5)	0.84	0.84
8	0.70(15)	0.73(5)	0.77(5)	0.69	0.70
16	0.5(1)	0.59(5)	0.62(5)	0.55	0.56
32	0.4(1)	0.50(5)	0.49(5)	0.46	0.46

finite contribution to the continuum energy gap in this limit, then we require an asymptotic behavior for the $\tilde{f}_l(u)$ given by

$$\tilde{f}_l(u) \to c_l u^{(l+1)/3} \quad \text{as} \quad u \to \infty \tag{58}$$

which would lead to a continuum energy gap

$$\frac{E}{g} = \sum_{l=0}^{\infty} \frac{c_l}{2} \left(\frac{g}{2m} \right)^{(4l+1)/3} . \tag{59}$$

The leading term $O[(g/m)^{1/3}]$ has the correct behavior as predicted by Eq. (14).

The series have been calculated for $\tilde{f}_l$ ($l=0,1,\ldots,6$) up to order u^{14} for the vector excited state and order u^{13} for the scalar excited state. Coefficients for the series $\tilde{f}_l(u)$ ($l=0,1,2,3$) are listed in Table IV for the two energy gaps. The first five coefficients of $\tilde{f}_0(u)$ can be obtained from the results of Carroll *et al.* [8] and were listed previously by Hamer [11]. The series for $\tilde{f}_0(u)$ is identical with that obtained from a lattice version of the nonrelativistic Schrödinger equation (12), as shown by Kenway and Hamer [21], which confirms that we should obtain at least the leading term in the nonrelativistic limit correctly by this procedure.

The series for $\tilde{f}_l(u)$ must now be extrapolated from the strong-coupling limit $u=0$ to the continuum limit $u \to \infty$. The same techniques were employed for this purpose as for the previous series in x. The only question is what to take as

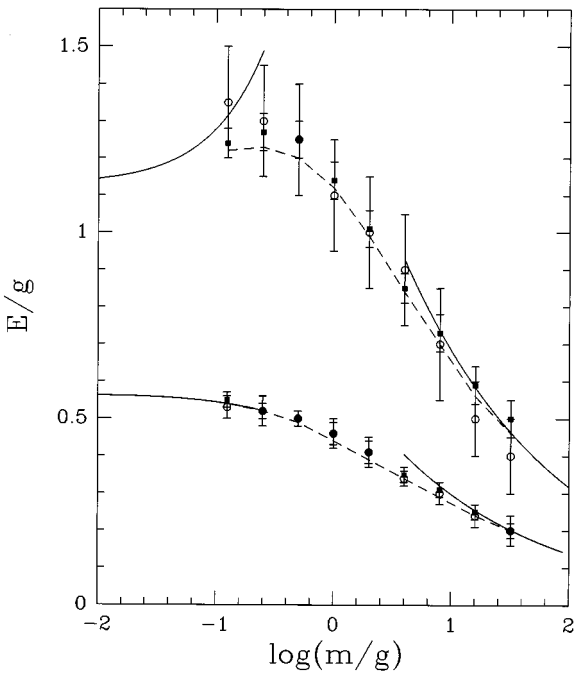

FIG. 8. Estimates of the bound-state energies E_i/g vs m/g for both the vector and scalar states. The open circles are our series estimates, the solid boxes are our finite-lattice estimates, the dashed line is the result of Mo and Perry, and the solid lines represent the asymptotic behavior in the limiting case $m/g \to 0$, and the nonrelativistic limit (log is to base 10).

TABLE IV. Series coefficients in u for the series $\tilde{f}_0$, $\tilde{f}_1$, $\tilde{f}_2$, and $\tilde{f}_3$ for the vector and scalar excited states.

n	$\tilde{f}_0$	$\tilde{f}_1$	$\tilde{f}_2$	$\tilde{f}_3$
		Vector excited state		
0	1.000000000000	0.000000000000	0.000000000000	0.000000000000
1	1.000000000000	$-5.000000000000\times10^{-1}$	$2.500000000000\times10^{-1}$	$-1.250000000000\times10^{-1}$
2	$-5.000000000000\times10^{-1}$	$-5.000000000000\times10^{-1}$	1.125000000000	-1.250000000000
3	$2.500000000000\times10^{-1}$	$5.000000000000\times10^{-1}$	$6.875000000000\times10^{-1}$	-3.437500000000
4	$-6.250000000000\times10^{-2}$	$-4.375000000000\times10^{-1}$	$-6.718750000000\times10^{-1}$	-1.375000000000
5	$-4.687500000000\times10^{-2}$	$2.500000000000\times10^{-1}$	$6.484375000000\times10^{-1}$	1.496093750000
6	$7.161458333333\times10^{-2}$	$-3.906250000000\times10^{-3}$	$-5.179036458333\times10^{-1}$	-1.298828125000
7	$-3.765190972222\times10^{-2}$	$-1.729600694444\times10^{-1}$	$2.191840277778\times10^{-1}$	$9.108886718750\times10^{-1}$
8	$-1.051613136574\times10^{-2}$	$1.898419415509\times10^{-1}$	$1.635357892072\times10^{-1}$	$-4.226029007523\times10^{-1}$
9	$3.595046055170\times10^{-2}$	$-6.325276692708\times10^{-2}$	$-4.165481755763\times10^{-1}$	$-1.153888466917\times10^{-1}$
10	$-2.772084302863\times10^{-2}$	$-9.454201278373\times10^{-2}$	$3.571410159515\times10^{-1}$	$5.813870214140\times10^{-1}$
11	$6.427749717514\times10^{-4}$	$1.602973539774\times10^{-1}$	$-1.180466277773\times10^{-2}$	$-7.371812834432\times10^{-1}$
12	$2.087420768938\times10^{-2}$	$-9.161565485249\times10^{-2}$	$-3.598007444620\times10^{-1}$	$3.895490578301\times10^{-1}$
13	$-2.186375166505\times10^{-2}$	$-4.596852371627\times10^{-2}$	$4.496844531498\times10^{-1}$	$3.420860280769\times10^{-1}$
14	$5.564121895836\times10^{-3}$	$1.366704793607\times10^{-1}$	$-1.603366455727\times10^{-1}$	$-9.530272768917\times10^{-1}$
		Scalar excited state		
0	1.000000000000	0.000000000000	0.000000000000	0.000000000000
1	3.000000000000	-1.500000000000	$7.500000000000\times10^{-1}$	$-3.750000000000\times10^{-1}$
2	$-5.000000000000\times10^{-1}$	-2.500000000000	4.125000000000	-4.250000000000
3	$-2.500000000000\times10^{-1}$	1.250000000000	3.562500000000	$-1.187500000000\times10^{1}$
4	$-6.250000000000\times10^{-2}$	$8.125000000000\times10^{-1}$	-4.046875000000	-4.187500000000
5	$4.687500000000\times10^{-2}$	$1.718750000000\times10^{-1}$	-2.632812500000	$1.437109375000\times10^{1}$
6	$7.161458333333\times10^{-2}$	$-3.554687500000\times10^{-1}$	$-9.993489583333\times10^{-2}$	8.261718750000
7	$3.765190972222\times10^{-2}$	$-4.944661458333\times10^{-1}$	2.158637152778	-2.571695963542
8	$-1.051613136574\times10^{-2}$	$-2.319607204861\times10^{-1}$	2.582842791522	$-1.177163357205\times10^{1}$
9	$-3.595046055170\times10^{-2}$	$1.738077799479\times10^{-1}$	$8.375302538460\times10^{-1}$	$-1.176848630552\times10^{1}$
10	$-2.772084302863\times10^{-2}$	$3.925574031877\times10^{-1}$	-1.691848582201	$-9.678567015095\times10^{-1}$
11	$-6.427749717514\times10^{-4}$	$2.711228939731\times10^{-1}$	-2.874944640017	$1.281942563814\times10^{1}$
12	$2.087420768938\times10^{-2}$	$-6.325043120993\times10^{-2}$	-1.598536929541	$1.730423290807\times10^{1}$
13	$2.186375166505\times10^{-2}$	$-3.223758205015\times10^{-1}$	1.178489577243	6.362423273963

a weak-coupling variable. No detailed weak-coupling analysis has been done in the nonrelativistic limit; but empirical tests on $\tilde{f}_0(u)$, making comparison with the exact results, appear to show that the best extrapolations are obtained using $z=1/u$ as weak-coupling variable. The results are shown in Figs. 9 and 10.

For the vector state, it can be seen that the integrated differential approximants converge down to $z\simeq0.2$, and the function behaves very smoothly in z, so that a very accurate extrapolation to the continuum limit is possible, giving

$$c_0^{\text{vector}}=1.618(2) \tag{60}$$

which compares well with the expected exact value of $1.617(=2^{4/3}\times0.642)$. Note that the series results are much better convergent than the finite-lattice results in this particular case.

The results for the scalar state are shown in Fig. 10, where it can be seen that the series approximants converge only down to $z\simeq0.7$, but the function is again quite smooth in z, so that a fairly reliable extrapolation may be made to the continuum limit, as confirmed by the finite lattice data. The resulting estimate is

$$c_0^{\text{scalar}}=3.73(3) \tag{61}$$

to be compared with the exact value of $3.71(=2^{4/3}\times1.473)$.

As soon as one tries to go beyond the leading order, however, some major problems arise. An example is shown in Fig. 11, which shows $\tilde{f}_1(u)/u^{2/3}$ for the vector state. It can be seen that the series approximants and the finite-lattice estimates agree very well down to very small values of z, and indicate a divergent behavior for this quantity. A Dlog Padé analysis of the series indicates that $\tilde{f}_1(u)$ behaves asymptotically more like u than $u^{2/3}$. Similar results are obtained for all the $\{\tilde{f}_l(u), l>0\}$, for both the vector and scalar states.

It therefore appears that assumption (58) is incorrect, and that the terms in Eq. (57) cannot be analyzed separately (beyond the leading order, at least). It is very likely that the limiting behavior of the energy gaps is nonuniform, and that by letting first $m/g\to\infty$, and then $a\to0$, we have taken the limits in the wrong order. This gives an incorrect result for the ground-state energy, for instance. It follows that expansion (59) is also incorrect; and in fact one would probably

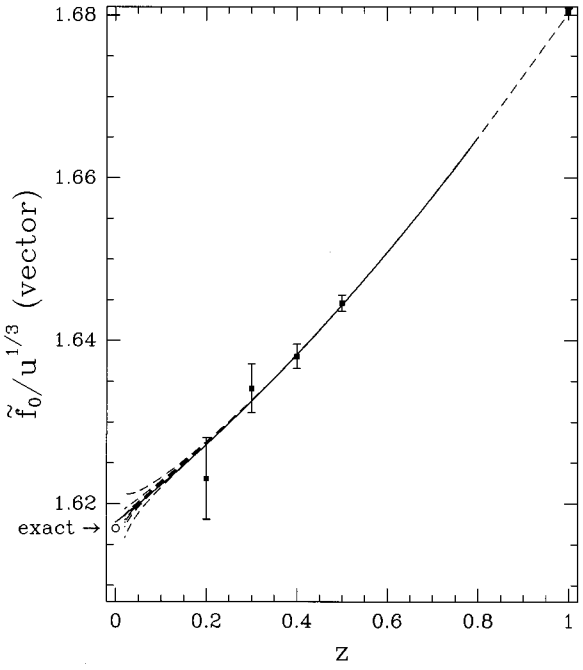

FIG. 9. Graph of the quantity $\tilde{f}_0/u^{1/3}$ as a function of $z=1/u$ for the vector excited state, notation as in Fig. 4. The solid line represents a polynomial fit in $1/u$ to the series results.

expect higher-order corrections to involve integer powers of (g/m), rather than $(g/m)^{4/3}$. It is an interesting puzzle how to obtain useful estimates of the higher-order corrections from the series data in these circumstances. At this stage, we have no answer to the puzzle.

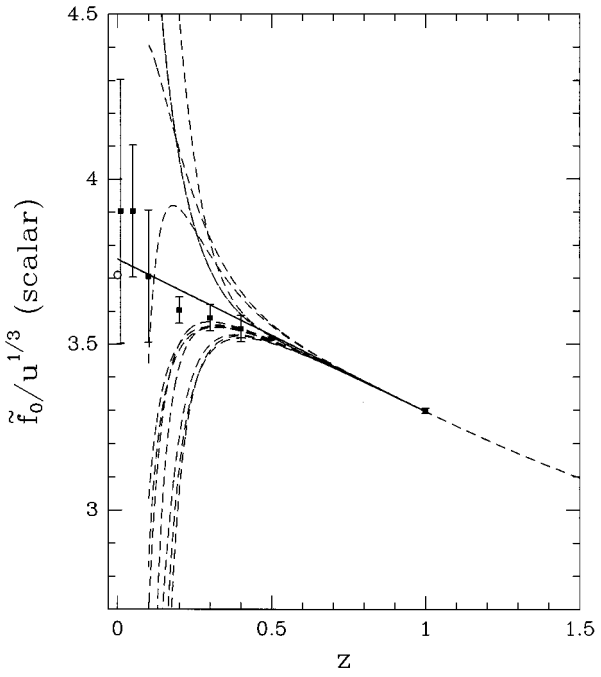

FIG. 10. Graph of the quantity $\tilde{f}_0/u^{1/3}$ as a function of $z=1/u$ for the scalar excited state, notation as in Fig. 4. The solid line is a linear fit in $z=1/u$ to the series data over the range [0.6–1] in z.

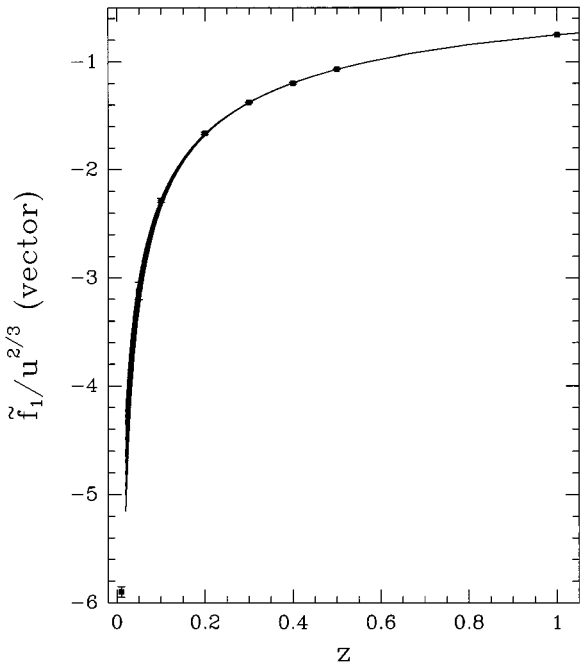

FIG. 11. Graph of the quantity $\tilde{f}_1/u^{2/3}$ as a function of $z=1/u$ for the vector excited state. The solid lines are integrated differential approximants to the series data, and the solid boxes are finite-lattice estimates.

IV. CONCLUSIONS

It has been shown that strong-coupling series expansions can deliver quite detailed and accurate information about the mass spectrum of the Schwinger model. Using integrated differential approximants or other methods, the series can be continued or extrapolated well into the weak-coupling regime, and then matched onto a weak-coupling form, which allows reasonably accurate estimates of the continuum limit. This has been confirmed by comparison with both finite-lattice data and exact results. At fixed, finite fermion mass the estimates for the lowest, vector excited state energy were accurate to about 5–10 %. For the next lowest, scalar excited state, the eigenvalue shows more structure at weak coupling, particularly for small m/g, and the continuum estimates are more qualitative, at about the 15–20 % level.

Estimates can also be obtained for the expansion coefficients of the continuum energy eigenvalues in powers of (m/g) about the zero-mass limit, $m/g\rightarrow 0$. These numerical estimates agree with the exact results of Carroll *et al.* [8], Vary *et al.* [9], and Adam [10], and extend them by one order. The series results for these coefficients have an accuracy equal to or better than that of the finite-lattice results.

A complementary expansion was attempted about the nonrelativistic limit, $m/g\rightarrow\infty$. Series estimates for the leading-order term of the nonrelativistic energy were extremely accurate in this limit, agreeing with the exact results to within 0.2% for the vector state, which is an order of magnitude better than could be obtained from fits to the finite-lattice data. Problems arose, however, for the higher-order correction terms. There appears to be a nonuniform limiting behavior in this case, and the natural structure of the strong-coupling series does not predict the correct limiting behavior. We have not resolved the puzzle of how to analyze

the series in this situation. It would be very interesting to compare the series data with more detailed analytic calculations in the nonrelativistic limit—we hope to address this problem in the future.

Finite-lattice techniques can also give accurate information about this model, as previously demonstrated by Crewther and Hamer [13] and Irving and Thomas [14]. Exact finite-lattice eigenvalues have been calculated for the equivalent spin Hamiltonian on lattices of up to $N=22$ sites, and then extrapolated to the bulk limit by polynomial fits in $1/N$. Fitting these estimates to a weak-coupling form, estimates of the continuum limit can be obtained which are accurate to about 5–10 % for both the vector and scalar states. This is actually worse than the accuracy of the old finite-lattice data of Crewther and Hamer [13].

The factor which hindered the finite-lattice calculations from giving even more accurate estimates was the large size of the finite-lattice corrections, $O(1/N^2)$, which were associated with the free boundary conditions. In retrospect, it might be better to choose periodic boundary conditions. This carries the penalty that the gauge field cannot be entirely eliminated, and one is left with one extra gauge degree of freedom corresponding to Coleman's background electric field or flux, which would have to be truncated in some fashion. The advantage would be that the finite-lattice corrections should be much smaller, and the finite-lattice sequence should converge more rapidly. With today's computers, one could probably expect to obtain virtually exact eigenvalues on lattices up to some 20 sites, and thus obtain a substantial improvement on previous finite-lattice calculations [13,14].

Generally speaking, the finite-lattice approach would be the method of choice for this particular model, and gives the most accurate results at fixed m/g. For models in higher dimensions, however, the finite-lattice approach is hardly feasible because of the huge proliferation of basis states with increasing lattice size. One would be forced to resort to Monte Carlo techniques, whose power is still rather limited for models with dynamical fermions. Our aim in this paper has been to show that the strong-coupling series approach can also give fairly accurate information about the spectrum of the Schwinger model. Having demonstrated the efficiency of these techniques, one can then go on to apply them with confidence to models in higher dimensions, where finite-lattice techniques are not practicable. It is worthy of note that the series approach actually outstripped the finite-lattice approach when it came to exploring the expansion of the vector mass gap about the small m/g and large m/g limits.

ACKNOWLEDGMENTS

This work forms part of a research project supported by a grant from the Australian Research Council.

APPENDIX

The full strong-coupling series up to order x^{10} are

$$\omega_0/N=-\frac{x^2}{1+2\,\mu}+\frac{3x^4}{(1+2\mu)^3}-\frac{2(29+20\mu)x^6}{(1+2\mu)^5(3+2\mu)}+\frac{(1443+2000\mu+700\mu^2)x^8}{(1+2\mu)^7(3+2\mu)^2}$$
$$-\frac{4(51\,093+126\,936\mu+117\,230\mu^2+47\,484\mu^3+7056\mu^4)x^{10}}{(1+2\mu)^9\,(3+2\mu)^3\,(5+2\mu)}, \tag{A1}$$

$$\omega_1-\omega_0=1+2\mu+\frac{2x^2}{1+2\mu}-\frac{2(5+2\mu)x^4}{(1+2\mu)^3}+\frac{4(59+68\mu+24\mu^2+4\mu^3)x^6}{(1+2\mu)^5\,(3+2\mu)}$$
$$-\frac{2(3313+6056\mu+3934\mu^2+1188\mu^3+216\mu^4+16\mu^5)x^8}{(1+2\mu)^7\,(3+2\mu)^2}+2(3\,578\,209+11\,359\,410\mu+14\,982\,934\mu^2$$
$$+10\,681\,694\mu^3+4\,498\,120\mu^4+1\,134\,808\mu^5+148\,448\mu^6-1888\mu^7-3712\mu^8-384\mu^9)$$
$$\times x^{10}[(1+2\mu)^9(3+2\mu)^3(5+2\mu)(7+2\mu)]^{-1}, \tag{A2}$$

$$\omega_2-\omega_0=1+2\mu+\frac{6x^2}{1+2\mu}-\frac{2(13+2\mu)x^4}{(1+2\mu)^3}+\frac{4(143+112\mu+4\mu^2-4\mu^3)x^6}{(1+2\mu)^5(3+2\mu)}$$
$$+\frac{2(-7905-11\,632\mu-4510\mu^2+28\mu^3+104\mu^4-16\mu^5)x^8}{(1+2\mu)^7(3+2\mu)^2}+(17\,055\,678+48\,682\,964\mu+54\,776\,904\mu^2$$
$$+30\,230\,052\mu^3+8\,173\,504\mu^4+987\,088\mu^5+157\,952\mu^6+74\,944\mu^7+14\,336\mu^8+768\mu^9)$$
$$\times x^{10}[(1+2\mu)^9(3+2\mu)^3(5+2\mu)(7+2\mu)]^{-1}. \tag{A3}$$

[1] J. Schwinger, Phys. Rev. **128**, 2425 (1962).
[2] J. Lowenstein and J. Swieca, Ann. Phys. (N.Y.) **68**, 172 (1971).
[3] A. Casher, J. Kogut, and L. Susskind, Ann. Phys. (N.Y.) **93**, 267 (1975).
[4] S. Coleman, Ann. Phys. (N.Y.) **101**, 239 (1976).
[5] S. Coleman, R. Jackiw, and L. Susskind, Ann. Phys. (N.Y.) **93**, 267 (1975).
[6] For a review, see H. X. He, C. J. Hamer, and J. Oitmaa, J. Phys. A **23**, 1775 (1990).
[7] T. Banks, L. Susskind, and J. Kogut, Phys. Rev. D **13**, 1043 (1976).
[8] A. Carroll, J. Kogut, D. K. Sinclair, and L. Susskind, Phys. Rev. D **13**, 2270 (1976).
[9] J. P. Vary, T. J. Fields, and H. J. Pirner, Phys. Rev. D **53**, 7231 (1996).
[10] C. Adam, Phys. Lett. B **382**, 111 (1996); **382,** 383 (1996).
[11] C. J. Hamer, Nucl. Phys. **B121**, 159 (1977).
[12] H. Bergknoff, Nucl. Phys. **B122**, 215 (1977).
[13] D. P. Crewther and C. J. Hamer, Nucl. Phys. **B170**, 353 (1980).
[14] A. C. Irving and A. Thomas, Nucl. Phys. **B215**, 23 (1983).
[15] T. Eller, H. C. Pauli, and S. J. Brodsky, Phys. Rev. D **35**, 1493 (1987).
[16] Y. Mo and R. J. Perry, J. Comput. Phys. **108**, 159 (1993).
[17] T. Tomachi and T. Fujita, Ann. Phys. (N.Y.) **223**, 197 (1993).
[18] M. N. Barber and C. J. Hamer, J. Aust. Math. Soc. B. Sppl. Math. **23**, 229 (1982).
[19] M. Henkel and G. Schütz, J. Phys. A **21**, 2617 (1988).
[20] For a review, see A. J. Guttmann, in *Phase Transitions and Critical Phenomena*, edited by C. Domb and J. L. Lebowitz (Academic, New York, 1989), Vol. 13.
[21] R. D. Kenway and C. J. Hamer, Nucl. Phys. **B139**, 85 (1978).
[22] C. J. Hamer, J. Oitmaa, and W. H. Zheng, Phys. Rev. D **45**, 4652 (1992).